Particle Acceleration in Near Critical Density Plasma

Y. J. Gu [1,2], Q. Kong[1], S. Kawata[2], T. Izumiyama[2], and T. Nagashima[2]

[1]*Applied Ion Beam Physics Laboratory, Key Laboratory of the Ministry of Education, Institute of Modern Physics, Fudan University, Shanghai 200433, People's Republic of China*

[2]*Department of Advanced Interdisciplinary Sciences, Utsunomiya University, Yohtoh 7-1-2, Utsunomiya 321-8585, Japan*

Abstract

Charged particle acceleration schemes driven by ultra intense laser and near critical density plasma interactions are presented. They include electron acceleration in a plasma channel, ion acceleration by the Coulomb explosion and high energy electron beam driven ion acceleration. It is found that under the near critical density plasma both ions and electrons are accelerated with a high acceleration gradient. The electron beam containing a large charge quantity is accelerated well with 23GeV/cm. The collimated ion bunch reaches 1GeV. The investigations and discussions are based on 2.5D PIC (particle-in-cell) simulations.

Keywords

laser-plasma interaction, particle acceleration, near-critical density plasma

1. Introduction

The rapid developments of laser technology make petawatt pulses applicable nowadays.[1,2] Such the ultra-intense pulse interacting with plasma to accelerate charged particles is one of the interesting topics in physics. When the intense laser pulse propagates through the plasma, it induces a wakefield to trap a part of electrons and accelerate them to a high energy. This is the so-called laser-wakefield-acceleration (LWFA) regime[3], which realizes a high acceleration gradient than that of conventional accelerators. The accelerated electron beam with a low emittance, small energy spread and large charge has been observed in experiments and simulations in recent years.[4] Generally, a relatively low density plasma, for example n_0~10^{-2}-$10^{-3}n_c$, is used to study the electron acceleration. Here, n_0 and n_c are the plasma initial and the critical densities, respectively. At the same time, an over-dense plasma with n_0~$10n_c$ is used to investigate the ion acceleration by laser-foil target interactions. High-energy ion beams are useful in many aspects such as cancer therapy[5], fusion ignition[6], particle physics[7], injection into conventional accelerators[8] and so on. Several regimes of ion acceleration have been proposed including target normal sheath acceleration

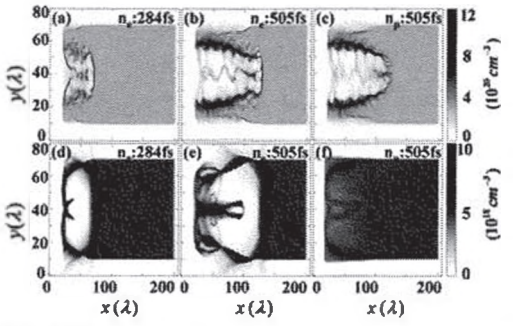

Fig.1 The comparison between the near-critical density case (CASE-A) and the lower density case (CASE-B). The electron density profiles at t=284fs and t=505fs are presented in (a) and (b) for CASE-A, while (d) and (e) for CASE-B, respectively. (c) and (f) depict the corresponding proton density distribution at t=505fs.

(TNSA),[9] shock wave acceleration,[10] radiation pressure,[11] laser break-out afterburner (BOA)[12] and Coulomb explosion[13]. Besides above, many other theoretical and experimental reports are

focusing on laser-plasma interaction induced charged-particle acceleration[14]. Usually, near critical density plasma is thought to be inappropriate to the particle acceleration. However, nowadays laser systems can produce ultra-short pulses with intensities above 10^{21}W/cm^2, with such a condition, many non-linear effects appear and some of these phenomena differ greatly from those of lower intensity lasers. In this paper, we present some of our researches on ultra intense laser interacting with near critical density plasmas. Through the scheme, remarkable electron acceleration and ion acceleration are realized[15].

2. Electron Acceleration in Plasma Channel

When ultra-intense laser pulses interact with a near critical density plasma, the phenomenon is quite different from the "bubble regime" under lower density plasma cases. In Fig. 1, two typical simulations for near critical density plasma $0.3n_c$ (Case-A) and lower density plasma $0.005n_c$ (Case-B) are presented to give the illustrations. Both simulations have the same laser parameters: a Gaussian laser pulse, which is linearly polarized in y direction with intensity $I\lambda^2 = 1.23\times10^{22} W/cm^2\cdot\mu m^2$ and radius $W_0=10\lambda$, incident from left in x direction and focused at the left plasma boundary at $x=20\lambda$, here $\lambda=1.053\mu$m is the pulse wavelength. The pulse amplitude rises as $a = a_0 \exp[-(\frac{t-\tau}{0.5\tau})^2]$, where $a_0=eE_0/(m_e\omega c)$ is the normalized amplitude and the pulse duration $\tau=35$fs. Instead of forming a closed electron bubble in Case-B (see Fig. 1 (e)), there exists a plasma channel in Case-A (see Fig. 1 (b)). Inside the channel, both the electron and proton density are much lower than the initial density n_0. A charge-balanced particle shell is surrounding the channel and forms a high density boundary. It is found that the laser pulse propagating through such the plasma channel is well confined. The radius of laser should be $W(z) = W_0\sqrt{1+(z/z_R)^2} = 12.6\lambda$ after propagating 245λ, where $z_R=\pi W_0^2/\lambda$ is the Rayleigh length. However the radius in Case-A is less than 10λ as shown in Fig. 1. According to the relativistic self-focusing condition $P > P_c \approx 17(\omega_0/\omega_p)^2(GW)$, the laser power threshold is inversely proportional to the plasma density. The self-focusing phenomenon is apparent in the near-critical density plasma in short distance about 100λ, since the higher plasma density and the ultra-intense laser lead it more easily to appear. The mechanism of this laser self-focusing effect is understood as the following: Because the transverse and longitudinal ponderomotive forces are nearly the same magnitude due to the ratio of $c\tau/W_0\approx1$, the background electrons are scattered in both transverse and longitudinal direction. Therefore it forms a dense electron wall, surrounding the laser pulse transversely, which confines the laser against the diffraction effect. Without the

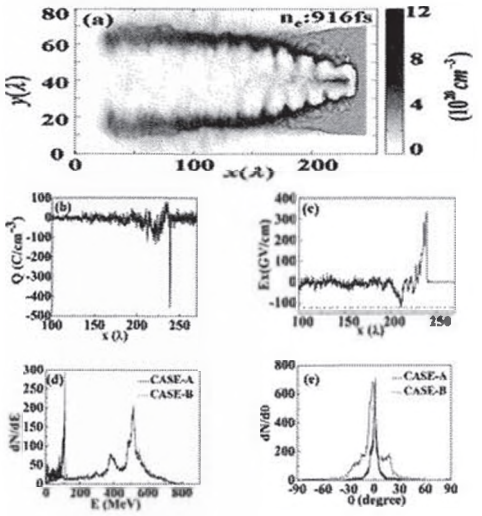

Fig. 2 Electron acceleration by the charge-separated field. (a) The density distribution of electron in Case-A at t=916fs. (b) and (c) show the charge density and longitudinal electric field along y=40λ. The dashed line in (c) depicts the minimum value of E_x. (d) and (e) present the energy spectrum and the angular distribution of the accelerated electron bunch, respectively. The solid line in (d) and (e) represents the value of Case-A, while the dashed line represents the quality of the accelerated electron beam at the same simulation time in Case-B.

diffraction, the laser maintains its intensity in the distance longer than the Rayleigh length, and the phenomenon do benefit to the electron acceleration by increasing the interaction length.

Figure 2 (a) depicts the electron density distribution at 916fs in Case-A. There is a high density electron shell driven by the longitudinal ponderomotive force, and it forms a negative charge region in front of the channel. There is a positive charge region behind the electron shell as shown in Fig. 2 (b). Such the charge distribution induces a longitudinal electric field which accelerates electrons violently. Since the initial density is near critical, the charge separated field is also intense with the maximum value about 122 GV/cm (see in Fig. 2 (c)). We present the energy and angular spectrum of the accelerated electron beam at 916*fs* in Figs. 2 (d) and (e) (black solid lines for Case-A and red dashed lines for Case-B), respectively. Within about 220 wavelengths, the peak energy of the electron beam in Case-A reaches about 512 *MeV*, *i.e.*, the effective accelerated gradient is about 23 GeV/cm. The peak energy in the lower density case (Case-B) is about 150*MeV*. The total charge of the accelerated electrons in Case-A is about 3nC/μm, while it is about 0.57nC/μm in Case-B. The accelerated beam in Case-A also shows good qualities with the energy spread $\Delta E / E \approx 0.062$, the angular divergence $\theta_{div} = \sqrt{\sum_{i=1}^{N} (\Delta\theta_i)^2 / N} \approx 0.158$ and the transverse emittance 0.52*mm·mrad* (which contains about 1.52nC/μm from 450MeV to 580MeV).

3. Ion Acceleration by Coulomb Explosion

In this section, we describe the ion acceleration on the rear side of the plasma channel by the Coulomb explosion effect. Since the electrons inside the channel have been expelled away by the laser pulse, the unneutralized ions begin expand under the Coulomb pressure. Some ions move transversely to form the channel shell, while some move forward to generate a shock wave, that excites the persistent Coulomb explosion. A part of ions move backwards and form a recoiled ion beam. Figures 3 (a) and (b) display the electron and ion density distributions at 3636 fs, respectively. An

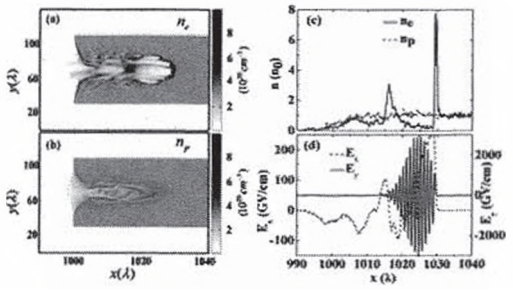

Fig. 3 (a) Electron and (b) proton density distributions at 3636fs. (c) Electron density on the central axis (y=70λ) (solid line) and the corresponding proton density (dashed line). (d) Longitudinal (dashed line) and transverse (solid line) electric field on the central axis.

electron cavity has been formed by the ultra-intense pulse and a significant amount of protons expand in the backward direction. The corresponding density profiles on the central axis, *i.e.* y=70λ, are plotted in Fig. 3 (c), while the transverse and longitudinal electric fields are shown in Fig. 3 (d). The electron density peak in front of the laser pulse (at about x=1030λ) indicates the electrons directly driven by the ponderomotive force. The second peak at about x=1017λ represents the electrons trapped and accelerated by the wakefield. Near the left plasma boundary, *i.e.* x=1000λ, the negative longitudinal electric field formed by the unbalanced charge distribution (several tens of GV/cm) accelerates the ions backwards violently. The number of the backward ejected protons are increasing with time evolution. This suggests that the Coulomb explosion continuously occurs with the pulse propagation inside the plasma, and such the mechanism has the potential to acquire large charge quantities. In Figs. 4 (a) and (b), we plot the time evolution of the recoiled proton beams' energy and angular spectra. The maximum and peak energy both increase with

time. At 3852 fs, that is, about 350 fs after the beginning of the Coulomb explosion, the peak energy and the maximum energy are 23.3 MeV and 63.9 MeV, respectively. After about 4000 fs, the peak energy increases to 45.4 MeV while the maximum energy increases to 191.3 MeV. The

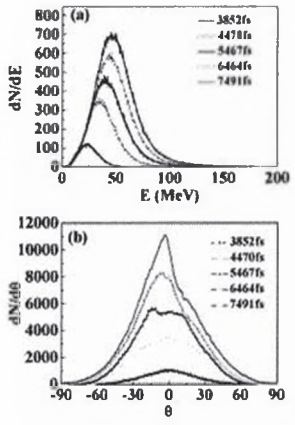

Fig. 4 The (a) energy and (b) angular spectra of the backwards accelerated ion bunch at t = 3852, 4470, 5467, 6464, and 7491fs.

angular spectrum indicates that the beam is also reasonably collimated. The energy spread, the angular divergence, and the transverse emittance of the ejected ion beam at 7491 fs are $\Delta E / E \approx 0.81$, $\theta_{div} = \sqrt{(\sum_{i=1}^{N} (\Delta\theta_i)^2)/N} \approx 0.47$ and $4/N\sqrt{\sum_{i=1}^{N}(y_i - \langle y\rangle)^2} \times \sqrt{\sum_{i=1}^{N}(\theta_i - \langle\theta\rangle)^2} \approx 71.1\, mm\, mrad$, respectively.

As we pointed out in the previous section, the laser pulse is effectively confined, when the plasma density is near critical and the intensity in the pulse center still rises after propagating over the depletion length. This suggests that the effective propagation length, *i.e.* the distance for the ion Coulomb explosion, is much longer than the depletion length. Therefore, even with the underdense plasma, the total quantity of acquired charge is fairly large, which can be estimated using the cylindrical model. At any moment t, the ions which can be backward-scattered, satisfy the condition: $v_{ion}(t - x/v_g) = x$, where x is the initial position of the ions, and v_{ion} and v_g are the average velocity of the ions and the pulse group velocity, respectively. The whole charge quantity at time t is $Q(t) = n_0 W_0 x$. We define $\zeta = \frac{v_{ion}}{v_{ion} + v_g}$, so that $x = \zeta v_g t$ and $Q(t) = n_0 W_0 v_g \zeta t$. Since the ion velocity increases from 0 to $0.3c$ during the acceleration process, it is reasonable to estimate the average velocity as

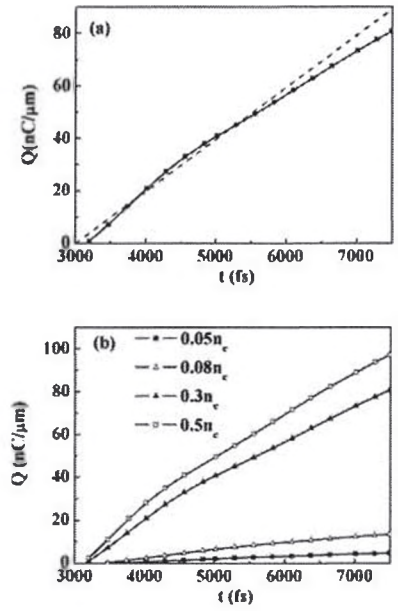

Fig. 5 (a) Time evolution of the acquired charge quantity with time evolution in the simulation (dotted line) and the corresponding results according to the theoretical estimate (dashed line). (b) Time evolution of the total acquired charge quantity with different initial plasma densities.

$v_{ion} = 0.15c$. In Fig. 5 (a) we present the acquired charge quantity as predicted by the above theoretical analysis (dashed line), compared to corresponding results from our simulations (black line/ square symbols). The small deviation between the two curves at the later time is caused by electron attraction effects, and ions' escaping from the bottom and top simulation boundaries. The total charge acquired in the simulation is about 80.74nC/μm, which is much larger than the current reported charge quantities acquired from other regimes. Bulanov

et al[16] undertook a study for a system with similar parameters and obtained ~1 GeV proton energy for acceleration in the forward direction. However, the charge quantity they acquired was only at a level of hundreds of pC, which is much less than the amount seen in our regime. Figure 5 (b) shows how the acquired charge quantity with the different initial plasma densities varies with time. The acquired charge is also approximately proportional to the initial plasma density.

4. LWFA Electron Beam driven Ion Acceleration

In this section, we focus on the proton acceleration driven by the charged-separated field, which is induced by the energetic laser wakefield accelerated (LWFA) electrons. From Fig. 6, one can see clearly about the proton beam generation. Before the LWFA electrons ejected out of the plasma, a small sheath field had appeared near the rear boundary of plasma (see Fig. 6 (a)), which is formed by the laser direct accelerated electrons. After the LWFA electrons ejected, as shown in Fig. 6 (b), the sheath field quickly increases and expands, the maximum amplitude reaches hundreds GV/cm, which is strong enough to drive protons. At this stage (Fig.6 (a)-(b)), the protons near the rear boundary started to move by the longitudinal field. The accelerated electrons at that time drift with a relativistic velocity $v \approx c$ relative to the background protons. The large gap between the velocity of protons and electrons is susceptible to induce the Buneman instability[17] and then efficiently accelerate ions. It should be noted that the most of the high energy protons come from the rear boundary of the plasma, rather than that of the proton bunch inside of plasma channel in Figs. 6 (a) and (b).

Different from the TNSA or BOA scheme in an overdense plasma, the leading electron bunch in this scheme is accelerated by the laser wakefield. We compare the electron beam quality in our simulation with that of a typical BOA results with the same laser parameters. The initial plasma density is $n_0=15n_c$ (2.6×10^{22}cm^{-3}) and plasma thickness is 0.8μm in the BOA case. We plot the energy and angular spectrum in Figs.

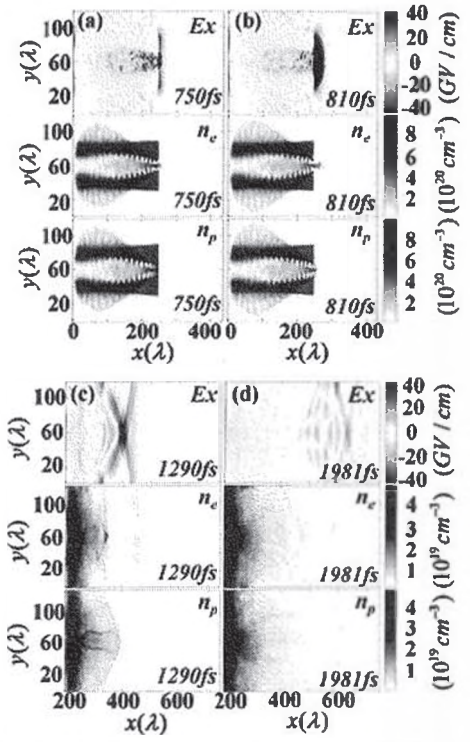

Fig. 6 The longitudinal electric field (E_x), the electron density distribution (n_e) and the proton density distribution (n_p) at t=750fs, t=810fs, t=1290fs and t=1981fs are plotted in (a), (b), (c) and (d), respectively.

7 (a) and (b), where the solid line represents the near-critical density case at 720fs, while the dashed line depicts the quality of the hot electrons, which penetrate through the target in the BOA case. One can find that the electron beam from the BOA case is generated by the direct laser acceleration process, the energy spectrum is almost the Maxwellian distribution with the highest energy about 250 MeV, and the angular distribution has two peaks around the cylindrical axis. On the other hand, the electron beam in the near-critical density case is quasi-monoenergetic with a peak energy about 300 MeV and the maximum energy becomes 800 MeV. The angular spectrum shows that this electron beam is also well collimated.

Figure 7 (c) depicts the longitudinal electrical

field along x=250λ, *i.e.* the right boundary of the plasma, at 750 fs. It suggests that the largest field is about 180 GV/cm and the strong region is tightly localized near the center. It is consistent with the spatial distribution of electron beam. Since the initial density of the plasma is the near critical, the charge separated field reaches hundreds GV/cm. Affected by such a strong field, the protons located near the center of right boundary are violently accelerated into the high energy in a short time and short distance. At the same time, the tightly focused size of the longitudinal field insures the accelerated proton beam to be well collimated. Near the right boundary of the target, a bunch of proton followed behind the electron beam is generated as shown in Fig. 6 (c).

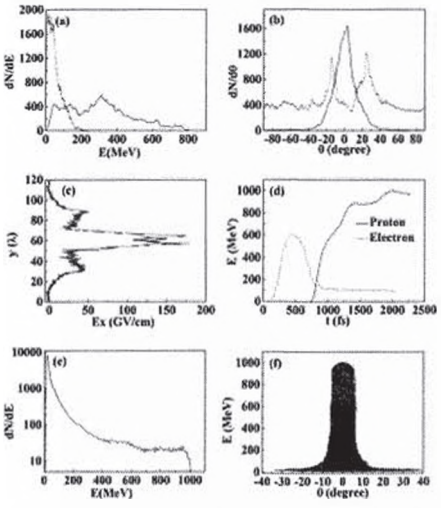

Fig. 7 (a) and (b) show the comparison between the energy spectrum and angular spectrum of overdense BOA case (dashed line) and the case of Fig.1 (solid line) respectively. (c) The longitudinal electric field along x=250λ at 750fs. The maximum energy of proton (solid line) and the energy of a typical leading electron (dashed line) with time evolution are presented in (d). (e) and (f) depicted the beam quality of the accelerated proton bunch at 2011fs. (e) The energy spectrum. (f) The energy angular related distribution.

The time evolution of the energy of a typical leading electron (dashed line) and the maximum energy of proton beam (solid line) are presented in Fig. 7 (d). The electron energy increases steadily before 500 fs and quickly decreases from 600 MeV to 100 MeV. After 750 fs, the decrease in the electron energy becomes slow and steady to about 100 MeV. On the other hand, the energy of protons increases violently since 750 fs and reaches 1 GeV at about 2000 fs. It is found the maximum energy of protons decreases slightly after 2011 fs, and at that time the leading electrons are ejected out of the simulation box at that time. But it is believed that the proton bunch is still accelerated by the electron beam, if the simulation area is larger enough. The protons begin to be accelerated around 750 fs, when the LWFA electrons are ejected out of the plasma; it means that the accelerated protons mainly come from the rear plasma boundary, as mentioned above. It is different from the magnetic vortex acceleration, by which the protons were accelerated inside of the plasma channel.

We present the energy spectrum and angular distribution of the proton bunch at 2011 fs, *i.e.* the last acceleration moment in our simulation in Figs. 7 (e) and (f). After the acceleration length about 400λ, the maximum energy of the proton bunch reaches 1 GeV; the effective acceleration gradient is about 32 GeV/cm. The scaling law of the TNSA acceleration mechanism suggests that with the laser intensity about 10^{22}W/cm^2 the energy of proton beam reaches hundreds of MeV. Since then, this scheme is much effective than that of TNSA. The total charge of the protons whose energy is larger than 50 MeV is about 4.05nC/μm. The total energy of the laser pulse in the simulation is about 37.3J/μm, then the energy transfer efficiency between the laser pulse and these high energy protons (E>50 MeV) is about 1.57%. If all the protons are taken into consideration, the energy laser-proton conversion efficiency is about 5.62%. From the energy angular related distribution, one can find that these high energy protons are well collimated between the angle $-10^{\circ} < \theta < 10^{\circ}$. The angular divergence of the proton bunch is

$\theta_{div} = \sqrt{\sum_{i=1}^{N} (\Delta\theta_i)^2 / N} \approx 0.144$ and the transverse emittance $7.706 mm \cdot mrad$.

5. Conclusions

In summary, ultra intense laser pulse interacting with near critical density plasma has been investigated. A laser self-focusing phenomenon and a steady plasma channel formation were found. The electrons captured by the laser wakefield inside the channel are accelerated by the large gradient. There exists both ion acceleration at the rear side by the Coulomb explosion and at the front side driven by the LWFA electron beam. This work is useful to laser-plasma charged particle acceleration scheme.

Acknowledgements

This work was partly supported by NSFC (No. 11175048), Shanghai Nature Science Foundation (No. 11ZR1402700), and Shanghai Scientific research innovation key projects No. 12ZZ011. Supports by China Scholarship Council, Shanghai Leading Academic Discipline Project B107, JSPS, MEXT, and CORE of Utsunomiya University are also acknowledged.

References

[1] Mourou G. Barty C, Perry M: Physics Today, **51**, 22 (1998)

[2] Perry D., Mourou G: Science. **264**, 917 (1994)

[3] Sprangle P, Esarey E, Ting A, and Joyce G, Appl. Phys. Lett. **53**, 2146 (1988)

[4] Mangles S. P. D. *et al.*, Nature **431**, 535-538 (2004); Geddes C. G. R. *et al.*, Nature **431**, 538-541 (2004); Faure J. *et al.*, Nature **431**, 541-544 (2004).

[5] Tajima T, J. Jpn. Soc. Therapy Rad. Oncol., **9**, 83 (1998); Bulanov S V, Khoroshkov V S, Plasma Phys. Rep., **28**, 453 (2002).

[6] Roth M. *et al.*, Phys. Rev. Lett., **86**, 436 (2001); Bychenkov V Yu *et al.*, Plasma Phys. Rep., **27**, 1017 (2001); Macchi A. *et al.*, Nucl. Fusion, **43**, 362 (2003); Honrubia J J. *et al.*, Phys. Plasmas, **16**, 102701 (2009).

[7] Esarey E, Schroeder C B and Leemans W P, Rev. Mod. Phys., **81**, 1229 (2009).

[8] Krushelnick K. *et al.*, IEEETrans. Plasma Sci., **28**, 1184 (2000).

[9] Wilks S. C. et al., Phys. Plasmas, **8**, 542 (2001).

[10] Ohsawa Y., Phys. Fluids, **28**, 2130 (1985); Silva L. O. *et al.*, Phys. Rev. Lett., **92**, 015002 (2004).

[11] Esirkepov T., *et al.*, Phys. Rev. Lett., **92**, 175003 (2004); Pegoraro F. and Bulanov S. V., Phys. Rev. Lett., **99**, 065002 (2007).

[12] Yin L. *et al.*, Laser Part. Beams, **24**, 291 (2006); Yin L. *et al.*, Phys. Plasmas, **14**, 056706 (2007).

[13] Last I. *et al.*, J. Chem. Phys., **107**, 6685 (1997); Bulanov S.V. *et al.*, Phys. Lett. A, **299**, 240 (2002).

[14] Leemans W. P. *et al.*, Nature **439**, 445 (2006); Malka V. *et al.*, Science **298**, 1596 (2002).

[15] Gu Y. J. *et al.*, Phys. Plasmas, **18**, 030704 (2011) ; Gu Y. J. *et al.*, Euro. Phys. Lett., **95**, 35001 (2011) ; Gu Y. J. *et al.*, Phys. Plasmas, **19**, 092308 (2012).

[16] Bulanov S. *et al.*, Phys. Plasmas **17**, 043105 (2010).

[17] Buneman O., Phys. Rev., **115**, 503 (1959).